the FEBS Journal

Mapping of the active site of glutamate carboxypeptidase II by site-directed mutagenesis

Petra Mlčochová[1,2]*, Anna Plechanovová[1,2]*,†, Cyril Bařinka[1,‡], Daruka Mahadevan[3], Jose W. Saldanha[4], Lubomír Rulíšek[1] and Jan Konvalinka[1,2]

1 Gilead Sciences and IOCB Research Centre, Institute of Organic Chemistry and Biochemistry, Academy of Sciences of the Czech Republic, Prague, Czech Republic
2 Department of Biochemistry, Faculty of Science, Charles University, Prague, Czech Republic
3 Department of Medicine, Hematology/Oncology, Arizona Cancer Center, Tucson, AZ, USA
4 National Institute for Medical Research, Division of Mathematical Biology, London, UK

Keywords
active site; metallopeptidase; mutagenesis; NAALADase; prostate specific membrane antigen

Correspondence
J. Konvalinka, Institute of Organic Chemistry and Biochemistry, Academy of Sciences of the Czech Republic, Flemingovo n. 2, 166 10 Praha 6, Czech Republic
Fax: +420 220 183578
Tel: +420 220 183218
E-mail: konval@uochb.cas.cz

*These authors contributed equally to this work

Present address
†College of Life Sciences, University of Dundee, UK
‡Center for Cancer Research, National Cancer Institute at Frederick, MD, USA

(Received 18 April 2007, revised 15 June 2007, accepted 11 July 2007)

doi:10.1111/j.1742-4658.2007.06021.x

Human glutamate carboxypeptidase II [GCPII (EC 3.4.17.21)] is recognized as a promising pharmacological target for the treatment and imaging of various pathologies, including neurological disorders and prostate cancer. Recently reported crystal structures of GCPII provide structural insight into the organization of the substrate binding cavity and highlight residues implicated in substrate/inhibitor binding in the S1′ site of the enzyme. To complement and extend the structural studies, we constructed a model of GCPII in complex with its substrate, *N*-acetyl-L-aspartyl-L-glutamate, which enabled us to predict additional amino acid residues interacting with the bound substrate, and used site-directed mutagenesis to assess the contribution of individual residues for substrate/inhibitor binding and enzymatic activity of GCPII. We prepared and characterized 12 GCPII mutants targeting the amino acids in the vicinity of substrate/inhibitor binding pockets. The experimental results, together with the molecular modeling, suggest that the amino acid residues delineating the S1′ pocket of the enzyme (namely Arg210) contribute primarily to the high affinity binding of GCPII substrates/inhibitors, whereas the residues forming the S1 pocket might be more important for the 'fine-tuning' of GCPII substrate specificity.

Human glutamate carboxypeptidase II [GCPII (EC 3.4.17.21)] is a membrane-bound metallopeptidase expressed in several tissues, including the prostate, brain, small intestine, and kidney [1–5]. Although the function of GCPII in prostate remains unclear, it is well known that this protein is overexpressed in prostate cancer [6–8]; hence, GCPII is a putative target for prostate cancer diagnosis and treatment [9–11].

In the brain, GCPII is expressed in astrocytes and cleaves *N*-acetyl-L-aspartyl-L-glutamate (NAAG), a neuropeptide, releasing *N*-acetyl-L-aspartate and free glutamate [12], the most potent excitatory

Abbreviations
AccQ, 6-aminoquinolyl-*N*-hydroxysuccinimidyl carbamate; NAAG, *N*-acetyl-L-aspartyl-L-glutamate; NAALADase, *N*-acetylated-α-linked-acidic dipeptidase; 2-PMPA, 2-(phosphonomethyl)pentanedioic acid; QM/MM, quantum mechanics/molecular mechanics; rhGCPII, recombinant human glutamate carboxypeptidase II (extracellular part, amino acids 44–750).

neurotransmitter in the central nervous system. Several potent inhibitors of GCPII act in a neuroprotective fashion in animal models of neurological disorders associated with high levels of glutamate, such as stroke and neuropathic pain [13–17]. GCPII also acts as a folate hydrolase and cleaves γ-linked glutamates from folyl-poly γ-glutamates, thus participating in the absorption of dietary folates in the small intestine [18].

For both activities of GCPII, the presence of oligosaccharides on the protein surface [19,20] and two zinc(II) ions complexed in the active site is essential. Based on the homology of GCPII with aminopeptidases from *Streptomyces griseus* and *Vibrio proteolytica* His377, Asp387, Glu425, Asp453, and His553 were proposed to coordinate the active-site zinc(II) ions and these predictions were later confirmed by mutational analysis experiments [21]. In the same study, Speno *et al*. [21] also targeted putative substrate binding residues (as predicted from the sequence alignment with the *Vibrio* aminopeptidase). The change in these residues negatively influenced but did not abolish GCPII activity.

Until recently, the only available structural data on GCPII consisted of models based on its homology with the transferrin receptor and members of M28 family [22–24]. However, structure–activity analysis using deletion mutants of the GCPII ectodomain showed that the putative protease domain itself supports neither proteolytic activity, nor the correct folding of the enzyme [25]. These biochemical observations were later rationalized by X-ray structures of the unliganded ectodomain of GCPII revealing that all three extracellular domains of GCPII cooperate to form the active site and substrate binding cavity of GCPII [26,27].

A more detailed insight into the active site was obtained by an analysis of crystal structures of the extracellular part of GCPII complexed with small molecules [28]. The structure with bound glutamate (Fig. 1) reveals that the previous predictions of its binding in the GCPII active site [21,23,26] were inaccurate. By contrast to the available models, L-glutamate is bound in the S1′ site via its α-carboxylate group, which forms a salt bridge with Arg210 and hydrogen bonds with the hydroxyl groups of Tyr552 and Tyr700. Furthermore, the γ-carboxylate of glutamate forms a strong salt bridge with Lys699 and the hydrogen bond with Asn257 [28] (Fig. 2A). Although the information about the S1′ pocket is rather detailed, very little is known about the architecture of the S1 site. Mesters *et al*. [28] suggest that the S1 pocket is defined by Asn519, Arg534, Arg536, Arg463, and Ser454.

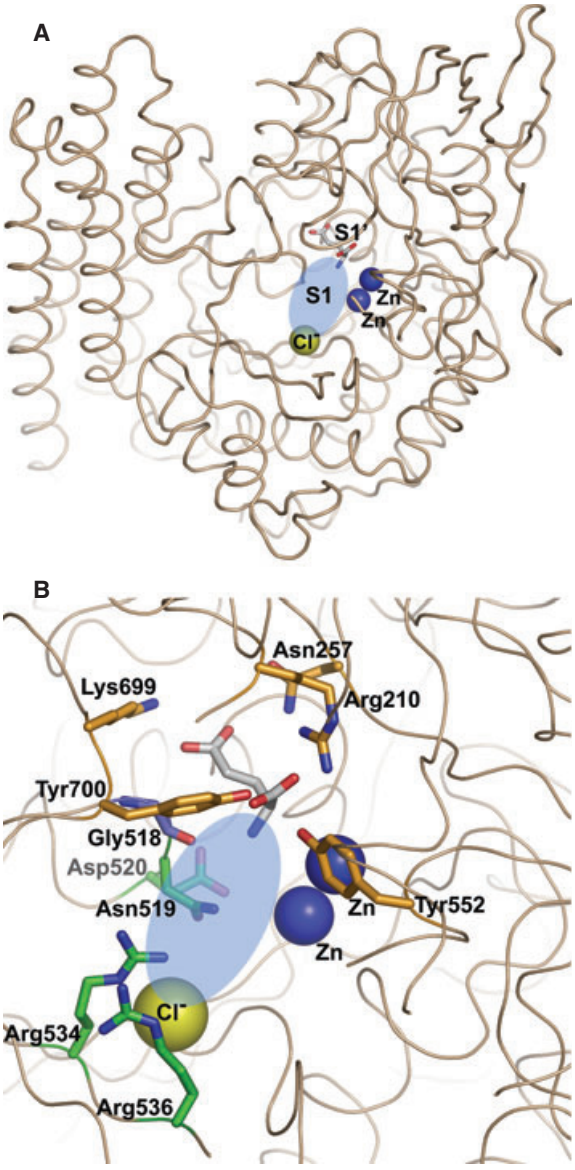

Fig. 1. Overall structure of the GCPII extracellular domain (designed from the structure of GCPII in complex with glutamate [28] using PYMOL molecular graphics system, version 0.97 (DeLano Scientific, San Carlos, CA, USA). (A) Ectodomain of GCPII in ribbon representation. Glutamate (the product of cleavage of the substrate NAAG) resides in the S1′ pocket of GCPII. The predicted S1 site is delineated by a blue oval near two zinc ions (blue spheres) and a chloride ion (yellow sphere). (B) A detailed look inside the active site of GCPII. The blue oval outlines the predicted GCPII S1 site. Amino acid residues defining the S1′ site are colored in orange, predicted S1 site residues are in green, and Gly518, which binds the free amino group of glutamate, is in slate color. Zinc ions (blue) and chloride ion (yellow) are depicted as spheres.

2-(Phosphonomethyl)pentanedioic acid (2-PMPA), the one of the most potent and specific inhibitors of GCPII published so far [29], includes a phosphonate

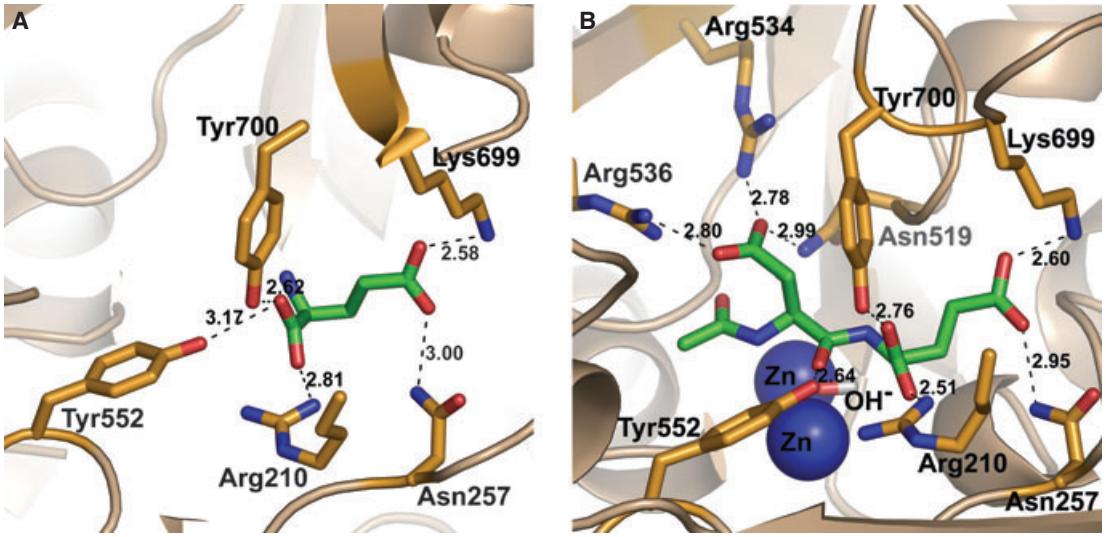

Fig. 2. Active site of GCPII with bound product (L-glutamate) and a natural substrate (NAAG). (A) Amino acid residues in the S1′ substrate binding pocket. L-glutamate (depicted here in green) is held in the active site via interactions with several amino acid residues (shown in orange). The α-carboxylate group of glutamate accepts hydrogen bonds from the hydroxyl groups of Tyr552 (distance of 3.17 Å) and Tyr700 (2.62 Å) and forms a salt bridge with Arg210 (2.81 Å). The γ-carboxylate group is recognized through an ionic interaction with Lys699 (2.58 Å) and through a hydrogen bond with the side-chain amide of Asn257 (3.00 Å). This picture was designed from the structure of GCPII in complex with glutamate [28] using PYMOL molecular graphics system, version 0.97 (DeLano Scientific). (B) The optimized QM/MM structure of NAAG bound in the active site of GCPII.The carbonyl group of L-aspartate from NAAG (depicted in green) accepts a hydrogen bond from the hydroxyl group of Tyr552 (distance 2.64 Å). The β-carboxylate group of L-aspartate forms strong salt bridges with two arginines, Arg534 and Arg536 (2.78 Å and 2.80 Å, respectively), and a hydrogen bond with Asn519 (2.99 Å). The structural arrangement of the glutamate part of NAAG within the S1′ pocket closely resembles the arrangement observed in the crystal structure of the rhGCPII/glutamate complex, with all principal interactions conserved. Zinc ions (blue) and the hydroxyl between them are also depicted. This picture was designed from the model of GCPII in complex with NAAG using PYMOL molecular graphics system, version 0.97 (DeLano Scientific).

group chelating the active site zinc ions and a glutarate moiety (pentanedioic acid) that binds to the glutamate recognition site of GCPII (the S1′ site) [28]. The majority of GCPII inhibitors have a glutarate moiety as a common denominator and differ only in their zinc-binding groups. Attempts to substitute the glutarate residue of the inhibitor led to significant decrease of inhibition potency *in vitro* [14,29–31]. The first successful improvement in efficiency by modifying the glutarate moiety of GCPII inhibitors was achieved by introducing the 3-carboxybenzyl group to the P1′ side chain of the inhibitor together with the sulfhydryl zinc-binding moiety [32].

To analyze the binding mode of the substrate/inhibitor to the active site of GCPII on a molecular level, we performed a structure–activity analysis of the residues participating in substrate/inhibitor binding in the S1′ pocket, as identified by X-ray structure analysis, and the residues predicted to participate in binding in the S1 pocket of the enzyme. The latter residues were identified both from the available crystal structures and the quantum mechanics/molecular mechanics (QM/MM) calculations of the substrate bound in the GCPII active site as reported here. Finally, the results of QM/MM calculations are used *a posteriori* to qualitatively elucidate the observed changes in k_{cat} and K_m values and provide some insight into the reaction mechanism of this prime pharmaceutical target.

Results

Site-directed mutagenesis

Based on the crystal structure of the recombinant human glutamate carboxypeptidase II (rhGCPII)/glutamate complex [28], as well as the QM/MM model of the rhGCPII/NAAG complex (see below), 12 mutations of amino acids delineating the substrate binding cavity of GCPII were designed and introduced into the GCPII ectodomain (rhGCPII; amino acids 44–750) using site-directed mutagenesis. Individual amino acid changes were created by modifying the rhGCPII sequence using two complementary oligonucleotide primers harboring the desired mutation (Table 1). The presence of individual mutations and the accuracy of the whole rhGCPII sequence were verified by dideoxynucleotide-terminated sequencing.

Table 1. Sequences of primers used for site-directed mutagenesis. Mutagenic bases are shown in bold.

Mutation	Nucleotide sequence (5′- to 3′)
R210A	GGGAAAGTTTTC**GCG**GGAAATAAGGTTAAAAATG
	CATTTTTAACCTTATTTCC**CGC**GAAAACTTTCCC
R210K	GGGAAAGTTTTCA**AG**GGAAATAAGGTTAAAAATGC
	GCATTTTTAACCTTATTTCC**CT**TGAAAACTTTCCC
N257D	GTCCAGCGTGGA**G**ATATCCTAAATCTGAATGG
	CCATTCAGATTTAGGATAT**C**TCCACGCTGGAC
G518P	GGATAAGCAAATTGGGATC**CCCA**AATGATTTTGAGGTG
	CACCTCAAAATCATT**TGGG**GATCCCAATTTGCTTATCC
N519D	GCAAATTGGGATC**C**GGA**G**A**C**GATTTTGAGG
	CCTCAAAATC**G**T**C**TCC**G**GATCCCAATTTGC
N519V	GGATAAGCAAATTGGGATC**C**GGA**GTT**GATTTTGAGGTGTTC
	GAACACCTCAAAATC**AAC**TCCG**G**ATCCCAATTTGCTTATCC
D520N	GCAAATTGGGATCTGGAAAT**AAT**TTTGAGGTGTTCTTC
	GAAGAACACCTCAAA**ATT**ATTTCCAGATCCCAATTTGC
R534L	GGAATTGCTTCAGGG**CTA**GCACGGTATACTAAAAATTGG
	CCAATTTTTAGTATACCGTGC**TAG**CCCTGAAGCAATTCC
R536L	GCTTCAGGCAGAGC**TCTG**TATACTAAAAATTGG
	CCAATTTTTAGTATA**CAGA**GCTCTGCCTGAAGC
Y552I	CAGCGGCTATCCACTG**ATT**CACAGTGTCTATGAAAC
	GTTTCATAGACACTGTG**AAT**CAGTGGATAGCCGCTG
K699S	CAAGCAGCCACAAC**TCA**TATGCAGGGGAGTC
	GACTCCCCTGCATA**TGA**GTTGTGGCTGCTTG
Y700F	GCAGCCACAACAAGT**TC**GCAGGGGAGTCATTCC
	GGAATGACTCCCCTGC**GA**ACTTGTTGTGGCTGC

Mutant protein expression and purification

Schneider's S2 cells were used for heterologous overexpression of wild-type rhGCPII (wt rhGCPII) as well as for the expression of rhGCPII mutants. Immunoblot analysis confirmed that all rhGCPII mutants were efficiently secreted into culture media (Fig. 3), suggesting correct protein folding. The expression levels of the individual rhGCPII mutants were comparable (in the range 0.8–1.7 $\mu g \cdot mL^{-1}$) and were approximately four- to eight-fold lower than wt rhGCPII expression (6 $\mu g \cdot mL^{-1}$; data not shown). In subsequent experiments, kinetic/inhibition parameters for the mutants with high specific activities (R534L, R536L, and Y552I) were determined using the conditioned media. wt rhGCPII and the remaining nine mutants, which exhibited lower specific activities, were expressed on a large scale and purified as described in the Experimental procedures.

Mutational analysis of the S1′ site

The previously reported crystal structure of the rhGCPII/glutamate complex [28] indicates that the α-carboxylate of the S1′-bound glutamate interacts with Arg210, Tyr552, and Tyr700, whereas the γ-carboxylate group is hydrogen bonded by the side chains of Asn257 and Lys699 (Fig. 2A). In the present study, the glutarate-binding residues of GCPII were mutated as follows: Arg210 (to Ala210 or Lys210), Asn257 (to Asp257), Tyr552 (to Ile552), Lys699 (to Ser699) and Tyr700 (to Phe700) (Tables 1 and 2).

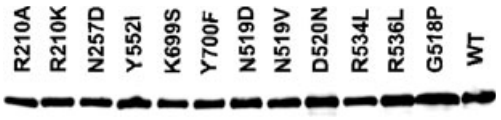

Fig. 3. Expression of individual mutant proteins. Recombinant protein expression was induced with 1 mM $CuSO_4$ in stably transfected S2 cell lines. Culture medium containing the expressed protein was harvested on the third day after induction. Proteins were resolved on a 10% SDS/PAGE gel, electroblotted onto a nitrocellulose membrane, and immunostained as described in Experimental procedures. The band intensities were recorded using a charge-coupled device camera. Amount of proteins applied: R210A (11 ng), R210K (11.9 ng), N257D(9 ng), Y552I (11 ng), K699S (8.4 ng), Y700F (8.2 ng), N519D (8.7 ng), N519V (9 ng), D520N(12 ng), R534L (8 ng), R536L (12 ng), G518P (13 ng). Purified wt rhGCPII (12.5 ng) is shown for comparison.

Table 2. Kinetic parameters of NAAG hydrolysis for wt and mutant forms of rhGCPII. Michaelis–Menten values (K_m) for NAAG hydrolysis were determined by a nonlinear least squares fit of the initial velocity versus concentration of the substrate and compared with wild-type enzyme. The concentrations of mutant proteins used for calculation of turnover number (k_{cat}) were determined by quantification from a western blot.

Mutation	K_m (μM)	k_{cat} (s^{-1})	k_{cat}/K_m ($mmol^{-1} \cdot s^{-1}$)
Wild-type [a,c]	1.15 ± 0.57	1.1 ± 0.2	957
Residues in the S1′ substrate binding site			
R210A[a,b]	294 ± 15	0.023 ± 0.001	0.08
R210K[a,b]	801 ± 124	0.130 ± 0.020	0.16
N257D[a,b]	68.10 ± 19.7	0.320 ± 0.080	4.70
Y552I[c,d]	0.15 ± 0.036	0.014 ± 0.001	93.3
K699S[a,b]	40.50 ± 22.9	0.270 ± 0.060	6.67
Y700F[a,b]	45.70 ± 6.6	0.075 ± 0.003	1.64
Residues in the predicted S1 substrate binding site			
N519D[a,b]	27.60 ± 0.300	0.078 ± 0.005	2.83
N519V[a,c]	0.67 ± 0.066	0.036 ± 0.001	53.7
D520N[a,c]	2.30 ± 0.180	0.007 ± 0.001	3.04
R534L[c,d]	0.14 ± 0.072	0.100 ± 0.040	714
R536L[c,d]	0.18 ± 0.005	0.010 ± 0.005	55.6
Residue binding free amino group of L-glutamate			
G518P[a,c]	2.20 ± 0.028	0.090 ± 0.020	40.9

[a] Kinetic parameters were measured using purified protein. [b] Kinetic parameters were determined by an HPLC assay. [c] Kinetic parameters were determined by a radioenzymatic assay. [d] Kinetic parameters were determined using the culture medium of the protein expressing cells.

The mutations of the glutarate-binding residues led to a dramatic increase in the Michaelis–Menten constant value (compared to wild-type), ranging from approximately 35-fold (for the K699S mutant) to an almost 700-fold increase for the R210K mutation (Table 2). The only exception was the Y552I mutant, which exhibited an eight-fold decrease in the K_m value. On the other hand, in most cases the mutations resulted in a relatively minor decrease in k_{cat} value, again with the exception of Y552I, which exhibited the largest decrease (approximately 80-fold) in k_{cat} detected in this series. The catalytic efficiencies of all the mutated proteins studied decreased by one to four orders of magnitude, which can be attributed mainly to the significant decrease in substrate binding (K_m values) (Table 2 and Fig. 4A).

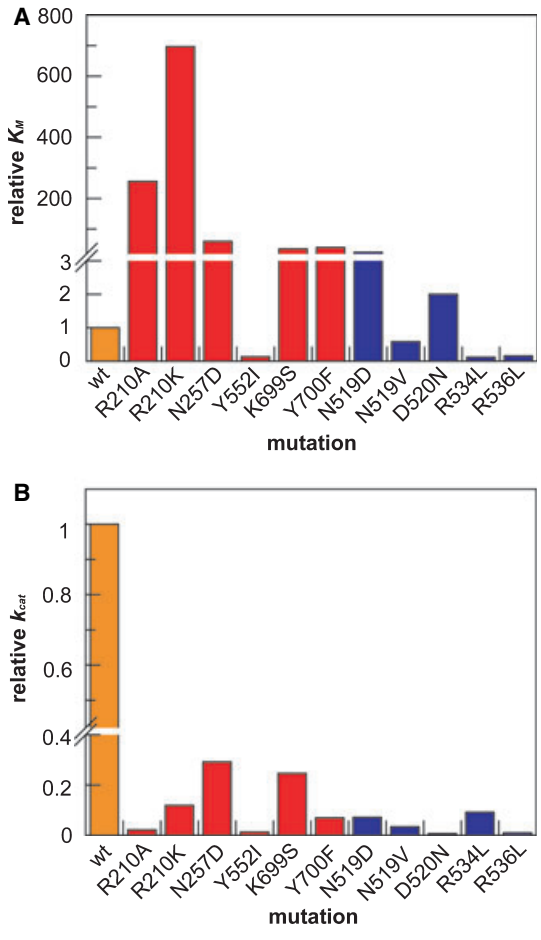

Fig. 4. Relative K_m and k_{cat} values for individual mutant proteins. Relative values of kinetic parameters of NAAG hydrolysis for mutant proteins with a substitution in the S1′ site are shown as red columns, whereas blue columns are used for proteins with a mutation in the predicted S1 pocket. (A) Relative K_m values. (B) Relative k_{cat} values.

A model of the rhGCPII/NAAG complex: identification of residues delineating the S1 pocket

QM/MM calculations of the rhGCPII/NAAG complex yielded the equilibrium structure corresponding to the NAAG moiety bound in the active site of GCPII prior to its hydrolytic cleavage. All the details of the model structure, including the partial charges in all atoms used in the MM part, can be found in the PDB file deposited in the Supplementary material. A detailed structure of the GCPII active site with NAAG bound is depicted in Fig. 2B.

The structural arrangement and the enzyme–substrate interactions within the S1′ pocket closely resemble the arrangement observed in the crystal structure of the rhGCPII/glutamate complex, with all principal (polar) interactions preserved. In the S1 pocket, Arg534, Arg536, and Asn519 interact with the aspartate side chain from NAAG, whereas Tyr552 forms a hydrogen bond with the peptide bond oxygen (Fig. 2B).

It can be observed that the NAAG molecule geometry differs from that of a free dipeptide and resembles the activated species. For example, the peptide bond hydrogen deviates from planarity by 25°. This is not quite surprising because the OH^- moiety coordinated between two zinc(II) ions is expected to initiate the hydrolytic cleavage of the NAAG peptide bond and the formation of the tetrahedral intermediate results in the nonplanarity of a peptide bond.

The structural aspects of the NAAG binding mode enable us to discuss the possible changes in the values of K_m caused by the amino acid substitutions. It is more difficult to utilize the model structure for discussions of k_{cat} values because these are directly related to the transition state structures and the corresponding free energy barriers, which are not yet available.

Mutational analysis of the S1 site

The model of the rhGCPII/NAAG complex suggests that GCPII most likely interacts with the N-terminal part of the substrate via the side chains of Asp453, Asn519, Arg534, and Arg536 (Fig. 2B). To verify this model experimentally, the N519D, N519V, R534L, and R536L mutants were constructed and kinetically characterized and the results are summarized in Table 2 and Fig. 4.

In general, mutations of the S1 residues interacting with the substrate led to a significant decrease in k_{cat} values (Fig. 4B), whereas the changes in K_m values were rather modest. Not surprisingly, the changes observed in the kinetic parameters were largely depen-

dent on the nature of the amino acid newly introduced. When Asn519 was mutated to aspartate, the N519D mutant exhibited a 24-fold increase in K_m compared to the wt rhGCPII. On the other hand, the Asn to Val mutation at the same position did not lead to a significant change in the K_m value. The corresponding k_{cat} values were approximately 14-fold (for N519D) and 30-fold (for N519V) lower than that of the wild-type enzyme. Both Arg534 and Arg536 were individually mutated to leucine. These mutations were unexpectedly associated with a moderate decrease in the K_m values as well as a pronounced decrease in the turnover number for both mutants.

Amino acid residues binding free amino group of L-glutamate

The free amino group of glutamate is bound through carbonyl oxygen of Gly518 and with a water molecule that is hydrogen-bonded to Tyr552. As discussed above, the mutation Y552I leads to the decrease of both the K_m and k_{cat} values. The mutation of Gly518 to Pro led to a slight increase of the K_m value and one order of magnitude decrease of the k_{cat} value (Table 2).

Analysis of inhibitor binding to the mutated proteins

Inhibition constants (K_I) for 2-PMPA [33], were determined for seven mutant proteins, and the data are summarized in Table 3. Compared with those of the wild-type enzyme, the K_I values for the rhGCPII mutants with S1′ amino acid substitutions were increased by two- to five orders of magnitude. The highest increase was observed for the R210A mutant protein, which showed a K_I value five orders of magnitude higher. Of the mutations outside the S1′ pocket, the N519D, N519V, and R534L mutations resulted in an increase in the K_I value compared to the wt rhGCPII (30-fold, 11-fold, and 2.5-fold, respectively).

Table 3. K_I values for 2-PMPA. Inhibition constants for 2-PMPA were measured using HPLC and radioenzymatic assays as described in Experimental procedures. *N*-acetyl-L-aspartyl-L-methionine was used as the substrate for wt rhGCPII, whereas NAAG was used for all the mutant proteins.

Mutation	K_I (nM)
Wild-type	0.18 ± 0.03
Residues in the S1′ substrate binding site	
R210A	22 000 ± 1,000
N257D	626 ± 46
K699S	32.7 ± 5.40
Y700F	49.7 ± 2.60
Residues in the predicted S1 substrate binding site	
N519D	5.6 ± 0.4
N519V[a]	1.8 ± 0.3
R534L[a]	0.5 ± 0.1

[a] K_I values were determined by a radioenzymatic assay.

Discussion

The present study aimed to analyze the binding pocket of human GCPII using molecular modeling and site-directed mutagenesis analysis. Guided by the previously determined crystal structure of GCPII, we set out to complement the available structural data by a functional analysis of the GCPII mutants. Additionally, the QM/MM calculations of the NAAG binding mode in the GCPII active site enabled us to predict the structure and enzyme–substrate interactions in the S1 binding site. Such a detailed information cannot be obtained from the crystal structure; however, the complete description of the reaction mechanism by QM/MM modeling is beyond the scope of the present study, and the structural insights obtained are used in the qualitative way.

The biochemical data clearly indicate that interactions in S1′ pocket are indispensable for high affinity substrate or inhibitor binding. In this respect, Arg210 is the most important residue. Somewhat surprisingly, the mutation R210K leads to dramatic increase of K_m and decrease of k_{cat}. Arg210 apparently fulfills a dual role in the architecture of the S1′ site. First, it interacts directly with an α-carboxylate of the C-terminal substrate residue, assuring GCPII selectivity as a carboxypeptidase. Second, it is important for maintaining productive architecture of the S1′ site of GCPII, including the positioning of the Tyr552 side chain. Despite similarities between lysine and arginine residues, the lysine side chain could not fully substitute Arg210 as the N-ε group, contrary to the arginine guanidinium group, can not simultaneously engage both the α-carboxylate of NAAG and the Tyr552 hydroxyl group. Consequently, it is likely that the R210K mutation leads to rearrangement of Tyr552 and/or active-site bound NAAG, resulting in observed changes in kinetic parameters of GCPII.

The importance of the S1′ subsite for the ligand binding is also documented by previously published structure-activity data on GCPII inhibitors showing that the glutarate part of various inhibitors, which presumably targets in the S1′ pocket [28], is very sensitive to any structural change [29,30,34]. Moreover, a change in the α-carboxylate group is more disruptive

than a change in the γ-carboxylate group [32,34,35]. The glutarate moiety is also present in 2-PMPA, one of the most potent inhibitors of GCPII published to date ($K_I = 0.3$ nM) [29], and the α-carboxylate group, which has been shown to interact with Arg210, renders this structural feature indispensable for potent inhibitor binding.

The only residue in the S1′ site which does not seem to be critical for substrate binding is Tyr552. The OH group of Tyr552 forms a weak hydrogen bond with the α-carboxylate group of C-terminal glutamate and with the carbonyl group of the Asp-Glu peptide bond (in the QM/MM model). Tyr552 could play a more important role in transition state stabilization, which might explain why the mutagenesis of this residue leads to such a dramatic decrease in k_{cat} value.

It should be noted that, in addition to polar interactions, there are also nonpolar interactions that might contribute to the substrate/inhibitor binding (Phe209, Leu428, C. Bařinka, unpublished results), which are not analyzed in this study.

The important role of the S1′ residues is also supported by the fact that all of them are conserved in the GCPII homolog GCPIII and in the mammalian GCPII orthologs (Table 4) and that the ability of these enzymes to bind NAAG is highly similar to that of GCPII [36] (M. Rovenská, K. Hlouchová, P. Šácha, P. Mlčochová, V. Horák, J. Zámeènik, C. Bařinka & J. Konvalinka, unpublished results). On the other hand, the GCPII homolog *N*-acetylated-α-linked-acidic dipeptidase L (NAALADase L), which does not cleave NAAG [37], has only two (out of five) of these residues conserved (Arg210 and Tyr552). It can be postulated that NAALADase L cannot bind NAAG with enough affinity for cleavage due to the absence of certain important residues in the S1′ site.

To identify the residues delineating the S1 binding pocket, a QM/MM analysis of the interaction between the enzyme and its natural substrate was performed. Previous inhibition studies revealed that the S1 pocket appears to be large, and a wide variety of substituents are tolerated at the N-terminus of a phosphonate or phosphinate analogue without a significant loss in inhibitor potency [34,38]. We have recently shown that the S1 pocket is critical for GCPII specificity (only Glu and Asp are tolerated in the P1 position of the *N*-acetylated substrate) [19]. In agreement with structure–activity relationship analysis, our findings confirm that the S1 pocket tolerates more variability and does not contribute substantially to affinity of the substrate binding.

Interestingly, the mutations of Arg534 and Arg536 lead to decreases in K_m. It can be speculated that the enzyme is able to compensate for the lost interaction of one arginine. The side chain of Arg536 adopts two different conformations in the crystal structure of ligand-free GCPII [27]. Additionally, when the crystal structures of GCPII complexes with glutamate, inhibitor GPI-18431, and phosphate are superimposed, both Arg534 and Arg536 appear to adopt different conformations depending on the bound ligand [28], suggesting that the enzyme might compensate for the lost ionic interaction in the S1 pocket by a rearrangement of the side chains of these amino acids.

Observed changes in GCPII kinetic parameters might not result only from disruption of the predicted direct interactions between enzyme and substrate; indeed, the amino acid substitutions might elicit unpredicted long-range rearrangements, possibly leading to major changes in the tertiary structure of the enzyme. These more complex effects could be documented by the unpredicted decrease in turnover number caused by the D520N mutation or by the different effects of substituting Asn519 with either Asp or Val. Speno *et al.* [21] reported mutations in amino acid residues located far from the active site of the enzyme, which nonetheless caused dramatic effects on the proteolytic activity (K499E, K500E). Furthermore, it should be noted that amino acid substitutions in the vicinity of the Zn ions (Arg210, Tyr552, Asn519, Asp520, and Arg536) have a more profound effect on k_{cat} in general

Table 4. The sequence alignment of human GCPII with its homologs and mouse and rat orthologs. GCPII was aligned with its homologs GCPIII, NAALADase L, and with orthologs, mouse and rat GCPII. Amino acid residues in the active site, which are changed compared to human GCPII, are depicted in bold.

	S1′					S1			
Residues	R210	N257	Y552	K699	Y700	N519	D520	R534	R536
Human GCPII	R	N	Y	K	Y	N	D	R	R
Human GCPIII	R	N	Y	K	Y	**S**	D	R	R
Human NAALADase L	R	**S**	Y	**V**	**V**	**S**	D	**D**	**A**
Mouse GCPII	R	N	Y	K	Y	N	D	R	R
Rat GCPII	R	N	Y	K	Y	N	D	R	R

than do substitutions farther away (Lys699, Asn257), most likely due to distortion of the coordination sphere of the active-site zincs.

Our results indicate that the binding of the glutarate part of the inhibitor in the S1′ pocket contributes to the inhibition effect of the specific inhibitor 2-PMPA [29]. This notion can be supported by the fact that the R210A mutant has the least ability to bind substrate and also exhibits the largest effect on inhibition by 2-PMPA. The decreased binding affinity of 2-PMPA is also observed for the N519D and N519V mutants. Although Asn519 does not directly interact with the glutarate moiety of the inhibitors, its side-chain amide forms a weak H-bond with one of the phosphonate oxygen atoms of 2-PMPA [39] contributing to the inhibitor binding.

Conclusions

In conclusion, we report a detailed analysis of the active site of glutamate carboxypeptidase II using site-directed mutagenesis as a tool. Amino acid residues important for substrate/inhibitor binding were determined from the crystal structures of GCPII with inhibitors and glutamate, and from a QM/MM model of the rhGCPII/NAAG complex. The results suggest that residues in the S1′ site are critical for substrate/inhibitor binding. It appears that amino acids in the S1 site are relevant for substrate turnover and may play a role in the enzyme's mechanism of action. The data presented here show that the glutarate part of inhibitor is essential for the affinity to the GCPII, whereas the S1 pocket of the enzyme allows for higher substrate/inhibitor diversity.

Experimental procedures

Reagents

SF900II medium, fetal bovine serum, pCoHygro plasmid, Hygromycin-B, Defined Lipid Concentrate, and Yeastolate Ultrafiltrate were purchased from Invitrogen (San Diego, CA, USA). Horseradish peroxidase conjugated goat secondary serum against mouse antibody, and SuperSignal West Dura Chemiluminiscence Substrate were obtained from Pierce (Rockford, IL, USA). AccQ Fluor reagent was obtained from Waters (Milford, MA, USA). Cupric sulfate ($CuSO_4$), EDTA, potassium phosphate, sodium chloride, sodium borate, L-glutamine, L-arginine, L-glutamate, NAAG, and D-glucose were purchased from Sigma (St Louis, MO, USA). Formic acid was obtained from Lachema (Brno, Czech Republic). 2-Amino-2-(hydroxymethyl)-1,3-propanediol was purchased from USB (Cleveland, OH, USA). Lentil lectin Sepharose was obtained from Amersham Biosciences (Uppsala, Sweeden) and ^{3}H-NAAG substrate was obtained from Perkin-Elmer (Boston, MA, USA).

Site-directed mutagenesis

Site-directed mutagenesis was carried out using the QuikChange Site-Directed Mutagenesis Kit (Stratagene, La Jolla, CA, USA). The pMTNAEXST plasmid [19] was used as a template, and each mutation was introduced by two complementary oligonucleotide primers harboring the desired mutation. The presence of individual mutations was verified by dideoxynucleotide-terminated sequencing. Nucleotide sequences of the primers used for individual amino acid changes are shown in Table 1.

Stable transfection of *Drosophila* S2 cells and large scale expression of mutant forms of rhGCPII

Transfection, stable cell line generation and expression of all mutant forms of rhGCPII were performed essentially as previously described [19] only the induction conditions were altered (to 1 mM $CuSO_4$).

Purification of mutant forms of rhGCPII

Mutant forms of rhGCPII were purified as previously described for wt rhGCPII [19] with minor modification for individual mutants described in the Supplementary material.

Western blotting and protein quantification

Proteins were resolved by SDS/PAGE, electroblotted onto a nitrocellulose membrane. probed with an GCPII mouse antibody (GCP-04, 1 mg·mL^{-1}; 1 : 5000) overnight at room temperature, and visualized and quantified using SuperSignal West Dura Chemiluminiscence Substrate [25].

Radioenzymatic assay

Radioenzymatic assay using ^{3}H-NAAG substrate (radiolabeled on the terminal glutamate) was performed as described previously [19], with minor modifications, using 20 mM Mops, 20 mM NaCl, pH 7.4 as a reaction buffer and the kinetic constants determined as previously described [19].

Kinetic constant determination by HPLC assay

To determine Michaelis–Menten kinetics, the NAAG concentration was varied to cover the range 0.3– 6 K_m. Typically, the substrate was mixed with 20 mM Mops, 20 mM NaCl, pH 7.4 and the reaction was started by the addition of

enzyme to a final volume of 120 μL. After a 15–30 min incubation at 37 °C, the reaction was stopped with 60 μL of stopping buffer (67 mM sodium borate, 33 mM EDTA, pH 9.2, containing 16 μM L-arginine as an internal standard). Released glutamate was derivatized by the addition of 20 μL of 2.5 mM AccQ Fluor reagent dissolved in acetonitrile. Thirty microlitres of the sample were then injected onto a Luna C18 column (250 × 4.6 mm, 5 μm, Phenomenex, Torrance, CA, USA) mounted to a Waters Aliance 2795 system equipped with a Waters 2475 fluorescence detector. Fluorescence was monitored at $\lambda_{EX}/\lambda_{EM} = 250/395$ nm.

Determination of inhibition constants

Measurements of inhibition constants for 2-PMPA were carried out with varying concentrations of the inhibitor while keeping the enzyme concentration fixed. The final enzyme concentrations used for individual mutants were: 12 nM for K699S, 10 nM for N257D, 150 nM for R210A, 38 nM for Y700F, 67 nM for N519D, 20 nM for N519V, 1 nM for R534L, and 32 nM for wt rhGCPII. Enzyme was preincubated with the inhibitor in reaction buffer (20 mM Mops, 20 mM NaCl, pH 7.4) for 10 min at 37 °C, and the reaction was started by the addition of NAAG to a final concentration of 60 μM (for mutant N519D), 100 μM (for mutants K699S, N257D, and Y700F), 600 μM (for mutant R210A) or 100 nM (for mutants N519V, and R534L). *N*-acetyl-L-aspartyl-L-methionine (50 μM) was used as a substrate for wt rhGCPII. Following a 20–40 min incubation at 37 °C, the reaction mixture was derivatized with AccQ Fluor reagent and product formation was quantified by HPLC with fluorimetric detection. K_I values for mutants N519V and R534L were obtained by using the radioenzymatic assay. The ratio of reaction rates of the inhibited reaction to the uninhibited reaction (v_i/v_0) was plotted against inhibitor concentration, and the apparent inhibition constant [$K_{I(app)}$] was determined from a nonlinear fit to Morrison's equation for tight-binding inhibitors [40] using GRAFIT software (Erithacus Software Ltd, Horley, UK). For mutant proteins N257D and R210A, tight-binding inhibition was not observed under the conditions used; therefore, IC_{50} values were determined. Inhibition constant (K_I) values were calculated using the Cheng and Prusoff relationship, which assumes a competitive inhibition mechanism. However, the mode of inhibition was not determined for either of the mutant proteins because it was assumed that the inhibition mechanism would not be changed by the mutations introduced.

Molecular modelling

QM/MM calculations were based on the 2.0 Å structure of GCPII in complex with inhibitor (S)-2-(4-iodobenzylphosphonomethyl)-pentanediodic acid (GPI-18431, PDB code 2C6C).

Prior to QM/MM modeling, three missing loops (12 amino acids in total, Thr334-Phe337, Trp541-Phe546, Lys655-Ser656) were added using the GCPII structure at 3.5 Å resolution (protein databank code 1Z8L) as a template [26]. Then, a total of approximately 100 atoms not resolved in side chains (i.e. missing from the crystal structure) were added using standard libraries. Finally, hydrogen atoms were added to the crystal structure, and the model, including hydrogen atoms, was solvated in a truncated octahedral box. The positions of all the hydrogen atoms, all nonhydrogen atoms added as described above, and solvent water molecules were then optimized by a 180-ps simulated annealing (i.e. molecular dynamics simulation, using constant volume and periodic boundary conditions) followed by a conjugate gradient energy minimization of their positions. We assumed the normal protonation state at pH 7 for all amino acids. For the His residues, the protonation status was decided from a detailed study of the hydrogen-bond network around the residue and the solvent accessibility. Thus, His82, 347, 377, 553, and 573 were assumed to be protonated on the $N^{\delta 1}$ atom; His112, 124, 295, 396, 475, 689, and 697 on the $N^{\varepsilon 2}$ atom; and His345 and 618 were considered to be protonated on both nitrogens.

The initial model for the QM/MM calculations of the rhGCPII/NAAG complex was obtained by replacement of the inhibitor with NAAG, such that the orientation and binding of the glutamate residue is identical to the crystal structure of the rhGCPII/glutamate complex, and the *N*-acetyl-L-aspartate part of the substrate is positioned in the cavity originally filled with the iodobenzyl part of inhibitor in the rhGCPII/GPI-18431 crystal structure. This structure has been subjected to QM/MM minimization. The quantum region consisted of side chains of Arg210, Asn257, His377, Asp387, Glu424, Glu425, Asp453, Asn519, Tyr552, His553, Lys699, Tyr700, two zinc(II) ions including the bridging H_2O/OH^- moiety and the molecule of NAAG. The details of QM and MM parts of QM/MM protocol are provided in the Supplementary material.

Acknowledgements

We thank Jana Starková for excellent technical assistance and Hillary Hoffman for critical proofreading of the manuscript. This work has been supported by grants from the Ministry of Education of the Czech Republic (Research Center for New Antivirals and Antineoplastics-1M0508 and Research Center for Complex Molecular Systems and Biomolecules LC 512).

References

1 Israeli RS, Powell CT, Corr JG, Fair WR & Heston WD (1994) Expression of the prostate-specific membrane antigen. *Cancer Res* **54**, 1807–1811.

2 Kinoshita Y, Kuratsukuri K, Landas S, Imaida K, Rovito PM Jr, Wang CY & Haas GP (2006) Expression of prostate-specific membrane antigen in normal and malignant human tissues. *World J Surg* **30**, 628–636.
3 Troyer JK, Beckett ML & Wright GL Jr (1995) Detection and characterization of the prostate-specific membrane antigen (PSMA) in tissue extracts and body fluids. *Int J Cancer* **62**, 552–558.
4 Dumas F, Gala JL, Berteau P, Brasseur F, Eschwege P, Paradis V, Lacour B, Philippe M & Loric S (1999) Molecular expression of PSMA mRNA and protein in primary renal tumors. *Int J Cancer* **80**, 799–803.
5 Lopes AD, Davis WL, Rosenstraus MJ, Uveges AJ & Gilman SC (1990) Immunohistochemical and pharmacokinetic characterization of the site-specific immunoconjugate CYT-356 derived from antiprostate monoclonal antibody 7E11-C5. *Cancer Res* **50**, 6423–6429.
6 Bostwick DG, Pacelli A, Blute M, Roche P & Murphy GP (1998) Prostate specific membrane antigen expression in prostatic intraepithelial neoplasia and adenocarcinoma: a study of 184 cases. *Cancer* **82**, 2256–2261.
7 Kinoshita Y, Kuratsukuri K, Newman N, Rovito PM, Kaumaya PT, Wang CY & Haas GP (2005) Targeting epitopes in prostate-specific membrane antigen for antibody therapy of prostate cancer. *Prostate Cancer Prostatic Dis* **8**, 359–363.
8 Ross JS, Sheehan CE, Fisher HA, Kaufman RP Jr, Kaur P, Gray K, Webb I, Gray GS, Mosher R & Kallakury BV (2003) Correlation of primary tumor prostate-specific membrane antigen expression with disease recurrence in prostate cancer. *Clin Cancer Res* **9**, 6357–6362.
9 Gong MC, Chang SS, Sadelain M, Bander NH & Heston WD (1999) Prostate-specific membrane antigen (PSMA)-specific monoclonal antibodies in the treatment of prostate and other cancers. *Cancer Metastasis Rev* **18**, 483–490.
10 Mincheff M, Altankova I, Zoubak S, Tchakarov S, Botev C, Petrov S, Krusteva E, Kurteva G, Kurtev P, Dimitrov V *et al.* (2001) In vivo transfection and/or cross-priming of dendritic cells following DNA and adenoviral immunizations for immunotherapy of cancer – changes in peripheral mononuclear subsets and intracellular IL-4 and IFN-gamma lymphokine profile. *Crit Rev Oncol Hematol* **39**, 125–132.
11 Todorova K, Ignatova I, Tchakarov S, Altankova I, Zoubak S, Kyurkchiev S & Mincheff M (2005) Humoral immune response in prostate cancer patients after immunization with gene-based vaccines that encode for a protein that is proteasomally degraded. *Cancer Immun* **5**, 1.
12 Robinson MB, Blakely RD, Couto R & Coyle JT (1987) Hydrolysis of the brain dipeptide N-acetyl-L-aspartyl-L-glutamate. Identification and characterization of a novel N-acetylated alpha-linked acidic dipeptidase activity from rat brain. *J Biol Chem* **262**, 14498–14506.
13 Chen SR, Wozniak KM, Slusher BS & Pan HL (2002) Effect of 2-(phosphono-methyl)-pentanedioic acid on allodynia and afferent ectopic discharges in a rat model of neuropathic pain. *J Pharmacol Exp Ther* **300**, 662–667.
14 Majer P, Jackson PF, Delahanty G, Grella BS, Ko YS, Li W, Liu Q, Maclin KM, Polakova J, Shaffer KA *et al.* (2003) Synthesis and biological evaluation of thiol-based inhibitors of glutamate carboxypeptidase II: discovery of an orally active GCP II inhibitor. *J Med Chem* **46**, 1989–1996.
15 Slusher BS, Vornov JJ, Thomas AG, Hurn PD, Harukuni I, Bhardwaj A, Traystman RJ, Robinson MB, Britton P, Lu XC *et al.* (1999) Selective inhibition of NAALADase, which converts NAAG to glutamate, reduces ischemic brain injury. *Nat Med* **5**, 1396–1402.
16 Zhou J, Neale JH, Pomper MG & Kozikowski AP (2005) NAAG peptidase inhibitors and their potential for diagnosis and therapy. *Nat Rev Drug Discov* **4**, 1015–1026.
17 Neale JH, Olszewski RT, Gehl LM, Wroblewska B & Bzdega T (2005) The neurotransmitter N-acetylaspartylglutamate in models of pain, ALS, diabetic neuropathy, CNS injury and schizophrenia. *Trends Pharmacol Sci* **26**, 477–484.
18 Pinto JT, Suffoletto BP, Berzin TM, Qiao CH, Lin S, Tong WP, May F, Mukherjee B & Heston WD (1996) Prostate-specific membrane antigen: a novel folate hydrolase in human prostatic carcinoma cells. *Clin Cancer Res* **2**, 1445–1451.
19 Barinka C, Rinnova M, Sacha P, Rojas C, Majer P, Slusher BS & Konvalinka J (2002) Substrate specificity, inhibition and enzymological analysis of recombinant human glutamate carboxypeptidase II. *J Neurochem* **80**, 477–487.
20 Barinka C, Sacha P, Sklenar J, Man P, Bezouska K, Slusher BS & Konvalinka J (2004) Identification of the N-glycosylation sites on glutamate carboxypeptidase II necessary for proteolytic activity. *Protein Sci* **13**, 1627–1635.
21 Speno HS, Luthi-Carter R, Macias WL, Valentine SL, Joshi AR & Coyle JT (1999) Site-directed mutagenesis of predicted active site residues in glutamate carboxypeptidase II. *Mol Pharmacol* **55**, 179–185.
22 Rawlings ND & Barrett AJ (1997) Structure of membrane glutamate carboxypeptidase. *Biochim Biophys Acta* **1339**, 247–252.
23 Rong SB, Zhang J, Neale JH, Wroblewski JT, Wang S & Kozikowski AP (2002) Molecular modeling of the interactions of glutamate carboxypeptidase II with its potent NAAG-based inhibitors. *J Med Chem* **45**, 4140–4152.
24 Mahadevan D & Saldanha JW (1999) The extracellular regions of PSMA and the transferrin receptor contain

an aminopeptidase domain: implications for drug design. *Protein Sci* **8**, 2546–2549.
25 Barinka C, Mlcochova P, Sacha P, Hilgert I, Majer P, Slusher BS, Horejsi V & Konvalinka J (2004) Amino acids at the N- and C-termini of human glutamate carboxypeptidase II are required for enzymatic activity and proper folding. *Eur J Biochem* **271**, 2782–2790.
26 Davis MI, BennettMJ, Thomas LM & Bjorkman PJ (2005) Crystal structure of prostate-specific membrane antigen, a tumor marker and peptidase. *Proc Natl Acad Sci USA* **102**, 5981–5986.
27 Barinka C, Starkova J, Konvalinka J & Lubkowski J (2007) A high-resolution structure of ligand-free human glutamate carboxypeptidase II. *Acta Crystallograph Sect F Struct Biol Cryst Commun* **63**, 150–153.
28 Mesters JR, Barinka C, Li W, Tsukamoto T, Majer P, Slusher BS, Konvalinka J & Hilgenfeld R (2006) Structure of glutamate carboxypeptidase II, a drug target in neuronal damage and prostate cancer. *EMBO J* **25**, 1375–1384.
29 Jackson PF, Cole DC, Slusher BS, Stetz SL, Ross LE, Donzanti BA & Trainor DA (1996) Design, synthesis, and biological activity of a potent inhibitor of the neuropeptidase N-acetylated alpha-linked acidic dipeptidase. *J Med Chem* **39**, 619–622.
30 Jackson PF, Tays KL, Maclin KM, Ko YS, Li W, Vitharana D, Tsukamoto T, Stoermer D, Lu XC, Wozniak K *et al.* (2001) Design and pharmacological activity of phosphinic acid based NAALADase inhibitors. *J Med Chem* **44**, 4170–4175.
31 Stoermer D, Liu Q, Hall MR, Flanary JM, Thomas AG, Rojas C, Slusher BS & Tsukamoto T (2003) Synthesis and biological evaluation of hydroxamate-based inhibitors of glutamate carboxypeptidase II. *Bioorg Med Chem Lett* **13**, 2097–2100.
32 Majer P, Hin B, Stoermer D, Adams J, Xu W, Duvall BR, Delahanty G, Liu Q, Stathis MJ, Wozniak KM *et al.* (2006) Structural optimization of thiol-based inhibitors of glutamate carboxypeptidase II by modification of the P1′ side chain. *J Med Chem* **49**, 2876–2885.
33 Rojas C, Frazier ST, Flanary J & Slusher BS (2002) Kinetics and inhibition of glutamate carboxypeptidase II using a microplate assay. *Anal Biochem* **310**, 50–54.
34 Kozikowski AP, Zhang J, Nan F, Petukhov PA, Grajkowska E, Wroblewski JT, Yamamoto T, Bzdega T, Wroblewska B & Neale JH (2004) Synthesis of urea-based inhibitors as active site probes of glutamate carboxypeptidase II: efficacy as analgesic agents. *J Med Chem* **47**, 1729–1738.
35 Oliver AJ, Wiest O, Helquist P, Miller MJ & Tenniswood M (2003) Conformational and SAR analysis of NAALADase and PSMA inhibitors. *Bioorg Med Chem* **11**, 4455–4461.
36 Hlouchova K, Barinka C, Klusak V, Sacha P, Mlcochova P, Majer P, Rulisek L & Konvalinka J (2007) Biochemical characterization of human glutamate carboxypeptidase III. *J Neurochem* **101**, 682–696.
37 Pangalos MN, Neefs JM, Somers M, Verhasselt P, van der Bekkers MHL, Fraiponts E, Ashton D & Gordon RD (1999) Isolation and expression of novel human glutamate carboxypeptidases with N-acetylated alpha-linked acidic dipeptidase and dipeptidyl peptidase IV activity. *J Biol Chem* **274**, 8470–8483.
38 Tsukamoto T, Flanary JM, Rojas C, Slusher BS, Valiaeva N & Coward JK (2002) Phosphonate and phosphinate analogues of N-acylated gamma-glutamylglutamate. Potent inhibitors of glutamate carboxypeptidase II. *Bioorg Med Chem Lett* **12**, 2189–2192.
39 Barinka C, Rovenska M, Mlcochova P, Hlouchova K, Plechanovova A, Majer P, Tsukamoto T, Slusher BS, Konvalinka J & Lubkowski J (2007) Structural insight into the pharmacophore pocket of human glutamate carboxypeptidase II. *J Med Chem* **50**, 3267–3273.
40 Morrison JF (1969) Kinetics of reversible inhibition of enzyme-catalysed reactions by tight-binding inhibitors. *Biochim Biophys Acta* **185**, 269–286.

Supplementary material

The following supplementary material is available online:

Doc S1. QM/MM procedure and quantum chemical calculation, purification of GCPII mutants.

Model S1. QM/MM model of rhGCPII/NAAG (.pdb format).

This material is available as part of the online article from http://www.blackwell-synergy.com

Please note: Blackwell Publishing is not responsible for the content or functionality of any supplementary materials supplied by the authors. Any queries (other than missing material) should be directed to the corresponding author for the article.